Prediction of a Giant Magnetoelectric Cross-Caloric Effect around a Tetracritical Point in Multiferroic $SrMnO_3$

Alexander Edström and Claude Ederer
Materials Theory, ETH Zürich, Wolfgang-Pauli-Strasse 27, 8093 Zürich, Switzerland

(Received 31 May 2019; accepted 25 March 2020; published 20 April 2020)

We study the magnetoelectric and electrocaloric response of strain-engineered, multiferroic $SrMnO_3$, using a phenomenological Landau theory with all parameters obtained from *first-principles*-based calculations. This allows us to make realistic semiquantitative and materials-specific predictions about the magnitude of the corresponding effects. We find that in the vicinity of a tetracritical point, where magnetic and ferroelectric phase boundaries intersect, an electric field has a huge effect on the antiferromagnetic order, corresponding to a magnetoelectric response several orders of magnitude larger than in conventional linear magnetoelectrics. Furthermore, the strong magnetoelectric coupling leads to a magnetic, cross-caloric contribution to the electrocaloric effect, which increases the overall caloric response by about 60%. This opens up new potential applications of antiferromagnetic multiferroics in the context of environmentally friendly solid state cooling technologies.

DOI: 10.1103/PhysRevLett.124.167201

Caloric effects in ferroic materials, where application or removal of external fields (magnetic, electric, or stress) can result in significant temperature changes, potentially allow for the development of clean and energy-efficient cooling technologies [1,2]. More recently, there has been growing interest in so-called multicaloric effects [3–7], where more than one type of caloric effect can occur simultaneously, possibly allowing to further optimize the total caloric response. Thereby, most specific studies have been focusing on combining either electrocaloric or magnetocaloric with elastocaloric effects, using applied stress or strain as an additional control parameter to enhance the overall caloric response [8–10] and/or to reduce irreversibility problems [11–14]. Recent work also discussed the importance of magnetism in stabilizing relevant ferroelectric phases in the context of the electrocaloric effect [15].

In contrast, multicaloric effects in (single phase) multiferroic materials with coexisting magnetic and ferroelectric (FE) orders have remained relatively unexplored [2,3], perhaps due to challenges in finding suitable materials. While such materials have received much attention, not only because of a broad fundamental interest, but also due to promises of technological applications [16,17], their practical usefulness is often hindered by low ordering temperatures or weak magnetoelectric (ME) coupling. Additionally, most magnetic ferroelectrics are in fact antiferromagnetic (AFM), which restricts their potential applications, since AFM order does not couple to magnetic fields. Here we show that an AFM multiferroic can, nevertheless, exhibit a large cross-caloric magnetic contribution to the electrocaloric effect (ECE) [18].

Since caloric effects are generally largest near the relevant phase transitions, a strong cross-caloric effect can be expected near a so-called tetracritical point (TCP) [19], where two ferroic critical temperatures coincide. Such a TCP was recently predicted in strained $SrMnO_3$ [20]; its existence can also be inferred from previous theoretical [21] and experimental [22–24] work. While perovskite structure bulk $SrMnO_3$ is a cubic paraelectric *G*-type antiferromagnet [25], it develops ferroelectricity under tensile epitaxial strain [21–24]. Thereby, the FE critical temperature increases strongly with strain [20], while the AFM Néel temperature is less affected, resulting in an intersection of the FE and AFM phase boundaries at a certain strain, and thus a TCP. Furthermore, since the Mn cation carries the magnetic moment and also takes part in the FE distortion, $SrMnO_3$ is expected to exhibit strong ME coupling, which is also implied by reports of a particularly strong spin-phonon coupling [26,27].

In this work, we explore ME coupling and cross-caloric response in $SrMnO_3$ by constructing a Landau-type model, considering all relevant magnetic and FE order parameters. We extract all parameters entering the free energy from first-principles-based calculations, allowing a realistic materials-specific description. We then apply the model to study ME coupling phenomena around the TCP in multiferroic $SrMnO_3$. We show that an electric field has a strong effect on the AFM order, shifting its critical temperature and increasing the corresponding order parameter, thereby drastically changing the entropy of the magnetic subsystem. This results in a huge magnetic cross-caloric contribution to the ECE, which is increased by about 60% due to the ME coupling.

$SrMnO_3$ under epitaxial strain is predicted to show a number of different AFM phases, including *G*, *C*, and *A* type [28], and possibly also ferromagnetic (FM) order at

large strains [20,21]. While there are three degenerate $\mathbf{q}$ vectors corresponding to each of the A- and C-type AFM orders within cubic symmetry, this degeneracy is broken in the strained case, and only $\mathbf{q} = \pi(0, 0, 1/c)$ (for A) and $\mathbf{q} = \pi(1/a, 0, 1/c)$ (for C) appear in the phase diagram of $SrMnO_3$ (in addition to FM and G) [20]. Each magnetic order parameter can couple to the polar order P that emerges under strain. Hence, we consider a Landau free energy of the form

$$\mathcal{F}_q = \frac{1}{2}a_P(T,\eta)P^2 + \frac{b_P}{4}P^4 + \frac{1}{2}a_q(T,\eta)M_q^2 + \frac{b_q}{4}M_q^4 + \frac{\lambda_q(\eta)}{2}M_q^2P^2 - EP, \quad (1)$$

for each magnetic order parameter $M_\mathbf{q} = (1/N)\sum_i^N e^{i\mathbf{q}\cdot\mathbf{R}_i}\langle S_i\rangle$, where $\langle S_i\rangle$ is the thermodynamic average of the normalized spin at site $\mathbf{R}_i$, and N is the number of spins. The strain and temperature dependence enters in the quadratic coefficients as $a_P = \alpha_P(T - T_0^P) + c_P\eta$ and $a_q = \alpha_q(T - T_0^q) + c_q\eta$. At each strain η, temperature T, and electric field E, the free energy $\mathcal{F}_q$ is minimized with respect to P and M_q, and the free energy is determined from $\mathcal{F} = \min_q(\min_{M_q,P}\mathcal{F}_q)$. The q which corresponds to the lowest free energy defines the equilibrium magnetic phase at that point in the phase diagram.

All parameters in Eq. (1) were determined from density functional theory (DFT) calculations and DFT-based effective Hamiltonian simulations [20,29]. The magnetic parameters and biquadratic ME coupling coefficients λ_q were obtained by mapping DFT total energy calculations on a Heisenberg Hamiltonian and extracting exchange interactions as functions of strain and FE distortions. The FE parameters were determined from the strain-dependent transition temperature and saturation polarization obtained from first-principles-based effective Hamiltonians [20], and from DFT-calculated elastic and electrostrictive constants.

We first consider the case without ME coupling and zero applied field and minimize the free energy in Eq. (1) for temperatures $0 \le T \le 600$ K and strains $0 \le \eta \le 5\%$. This results in the phase diagram shown in Fig. 1, which largely agrees with our previous study using microscopic *first-principles*-based Hamiltonians [20,40]. For small T and η, there is a G-AFM paraelectric (PE) phase, while at approximately 2% strain there is a transition into a FE region and also a change to C-AFM order. For large strain and low temperatures, an A-AFM FE region appears. We note that the ferromagnetism that has been predicted for large strains is only stabilized due to its coupling to the FE order [20], which is not yet included in our free energy. Most notably, the phase diagram in Fig. 1 reveals a TCP, where the magnetic and FE critical temperatures coincide, within the region with C-AFM order at $\eta_{\text{tcp}} = 2.63\%$ and $T_{\text{tcp}} = 162$ K. As also discussed in Ref. [20], the calculated

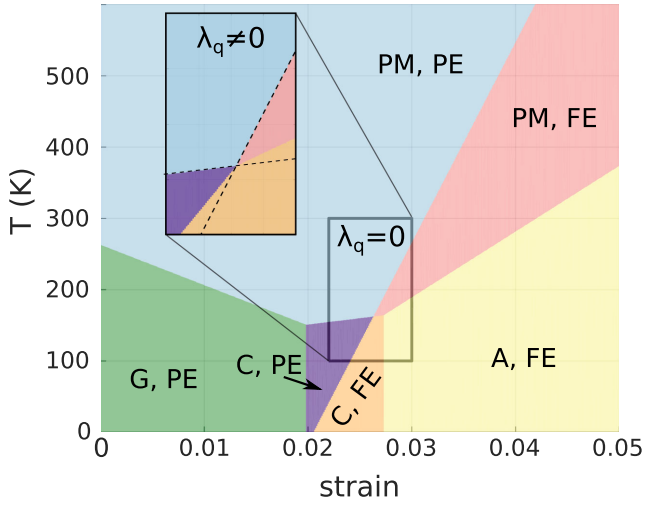

FIG. 1. Ferroic phase diagram of $SrMnO_3$ at zero applied field without ME coupling ($\lambda_q = 0$). The inset shows the effect of nonzero ME coupling around the TCP. The dashed lines in the inset indicate the FE-PE and the C-paramagnetic (PM) phase boundaries with $\lambda_q = 0$.

magnetic transition temperatures as function of strain agree well with those measured by Maurel *et al.* [41], indicating that our calculations yield a realistic semiquantitative description of the ferroic phase diagram of $SrMnO_3$.

Next, we include the strain-dependent ME coupling parameters, λ_q. We find that the lowest order biquadratic coupling in Eq. (1) is insufficient to describe the variation of the exchange couplings for large polarization [29], which occurs in the region of the phase diagram with large strain and low temperatures. A satisfactory description of this region would require coupling terms of higher order in P, which, however, requires additional higher order terms to guarantee stable, physical solutions, and thus more parameters in the free energy. In the following, we therefore focus on the part of the phase diagram which is most interesting in the present context, i.e., the region around the TCP, where both order parameters are small [42].

For the C-AFM order, relevant around the TCP, we find a negative ME coupling, which varies relatively weakly with strain. Previously, a positive ME coupling coefficient λ_G has been found for cubic $Sr_{1-x}Ba_xMnO_3$ [44,45], meaning that G-AFM and FE order couple unfavorably. This is consistent with our results [29]. However, we also find that the coupling coefficients change with magnetic order and strain.

The zero field phase diagram for the region $2.2\% \le \eta \le 3.0\%$ and $100\text{ K} \le T \le 300$ K, now including ME coupling, is shown in the inset of Fig. 1. One drastic effect of the coupling is that it suppresses the A-AFM region. This is because λ_A is found to be strongly positive and A-AFM only appears in the FE region, where it is highly unfavored by the coupling, while C-AFM is favored. In contrast, the coupling does not alter the position of the TCP, since both

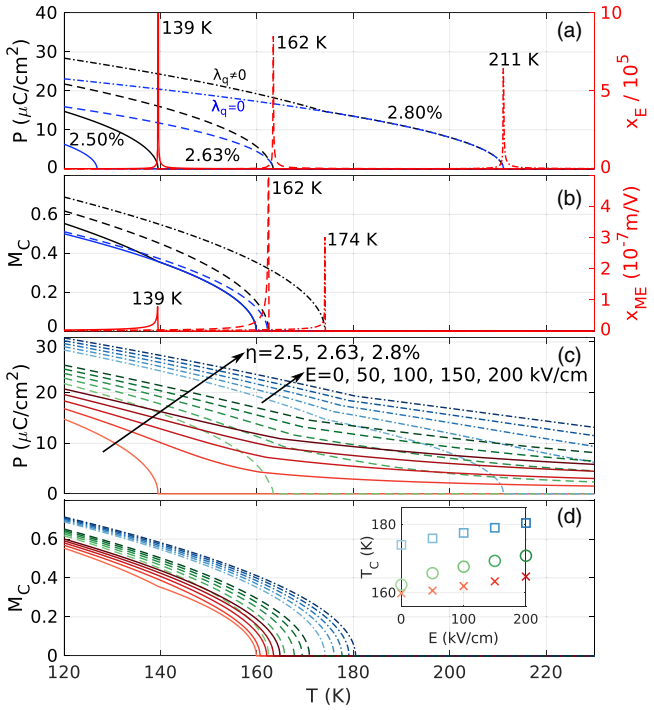

FIG. 2. (a) and (b) Order parameters (black, left) and susceptibilities (red, right) as functions of temperature for strains of 2.5% (solid line), 2.63% (dashed line), and 2.8% (dashed dotted line). (a) Electric polarization and susceptibility, (b) magnetic order parameter, and ME susceptibility. Order parameters for zero ME coupling are shown in blue. (c) and (d) Temperature dependence of FE (c) and magnetic (d) order parameters for strains of 2.5% (red solid lines), 2.63% (green dashed lines), and 2.8% (blue dashed dotted lines) with applied electric fields of 0, 50, 100, 150, and 200 kV/cm. The darker colors correspond to larger fields. The inset in (d) shows T_c^C as a function of E, with color coding corresponding to the main plot.

M_C and P, and thus the effect of the coupling term, vanish at this point. Away from the TCP, the upper of the two ordering temperatures also remains unaltered, while the lower one is increased by the negative ME coupling. This can also be seen from Figs. 2(a) and 2(b), which show the temperature dependence of the FE polarization P and the C-AFM order parameter M_C, both with (black) and without (blue) ME coupling, for three different strain values. At $\eta = 2.80\%$ (where $T_c^C < T_c^P$), T_c^P is unaffected, while the magnetic order changes from A to C with an increase in ordering temperature from $T_c^A = 170$ to $T_c^C = 174$ K. Additionally, the coupling enhances the polarization below T_c^C producing a kink in $P(T)$. Analogous behavior, but with the roles of P and M_C exchanged, is observed at $\eta = 2.50\%$ (where $T_c^C > T_c^P$). Here, the coupling does not alter T_c^C, while it shifts T_c^P from 127 to 139 K, and produces a kink in $M_C(T)$ at T_c^P. At $\eta_{\text{tcp}} = 2.63\%$, the coinciding critical temperatures are unaltered by the coupling term, however, below $T_{\text{tcp}} = 162$ K both order parameters are enhanced compared to the case with $\lambda_q = 0$. This behavior is consistent with the general phenomenological theory outlined in Ref. [7], where it was also shown that both transitions remain second order if $\lambda_q^2 < b_q b_P$ (or if $\lambda_q > 0$). According to our results this condition is fulfilled for every magnetic order and strain considered.

The zero-field electric susceptibility $\chi_E = (dP/dE)|_{E=0}$ (for $\lambda_q \neq 0$), is also plotted in Fig. 2(a). As expected, this susceptibility diverges at the FE transitions. Additionally, the ME susceptibility

$$\chi_{\text{ME}} = \left.\frac{dM_q}{dE}\right|_{E=0} = -\frac{\lambda_q P}{b_q M_q}\chi_E \tag{2}$$

is plotted in Fig. 2(b). This quantity describes the magnetic response to an applied electric field and is nonzero only in the multiferroic regions of the phase diagram (where $M_q \neq 0$ and $P \neq 0$). The ME susceptibility then diverges at the lower of the two transition temperatures, either because χ_E diverges if the FE transition is lower, or because $M_q \to 0$ if the magnetic transition is lower. The divergence is particularly pronounced at η_{tcp}, where χ_E diverges simultaneously as $M_q \to 0$, causing χ_{ME} to diverge as $(T_c - T)^{-1}$ instead of $(T_c - T)^{-1/2}$ when the relevant critical temperature T_c is approached from below [46].

We now discuss the effect of applying an electric field. In Figs. 2(c)–2(d), the FE and magnetic order parameters are plotted as functions of temperature for the previously discussed strain values and various applied electric fields. As expected, an electric field induces a nonzero electric polarization at all temperatures, decreasing towards high T, and thus removes the second order FE transition. The effect on the magnetic order parameter is markedly different. While the electric field enhances also M_C, because $\lambda_C < 0$, the magnetic order parameter still shows a second order transition, and is identically zero above the corresponding transition temperature. The magnetic transition temperature is, however, electric field dependent and the inset of Fig. 2(d) shows T_c^C as a function of applied electric field. The increase in T_c^C with E appears close to linear, and an applied field of 100 kV/cm increases T_c^C by 2.1 K for $\eta = 2.5\%$, by 5.3 K for $\eta_{\text{tcp}} = 2.63\%$, and by 3.5 K for $\eta = 2.8\%$. The largest effect of the electric field on T_c^C is thus found at η_{tcp}.

We note that $SrMnO_3$ is not a linear ME material. Nevertheless, to get a better idea of the magnitude of the electric field effect on M_C, one can see from Fig. 2(d) that an electric field of 50 kV/cm alters M_C by about 0.15 at the TCP. Considering a Mn magnetic moment of $3\mu_B$, one can estimate an effective ME coefficient of $\alpha_{\text{eff}} = (\Delta M/\Delta E) = 15 \times 10^{-3}\ \Omega^{-1}$, which is 4 orders of magnitude larger than that found in conventional linear magnetoelectrics such as Cr_2O_3 [47,48].

Based on the electric field response of both FE and magnetic order parameters, we now address the ECE in

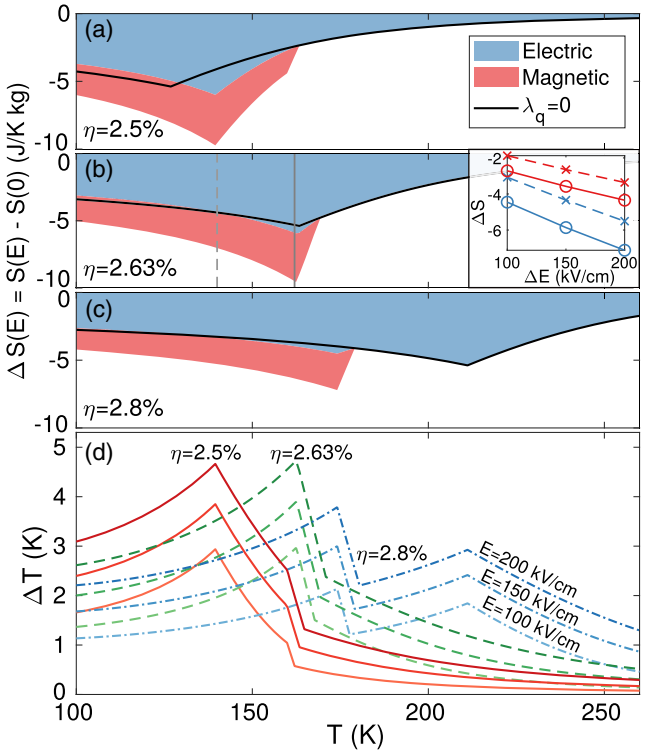

FIG. 3. The ECE as a function of temperature. (a)–(c) The isothermal entropy change, as a field of 150 kV/cm is applied, for strains of 2.5%, 2.63%, and 2.8%, respectively. (b) Contains an inset showing the field dependence at $T = 140$ (dashed) and $T = 162$ K (solid). The total entropy change is decomposed into magnetic (red) and electric (blue) contributions. Additionally, the ECE corresponding to $\lambda_q = 0$ is shown (black line). (d) Estimates of the adiabatic temperature changes for the same strains, and applied electric fields of 100, 150, or 200 kV/cm.

$SrMnO_3$. Because of the negative ME coupling, an applied electric field has an ordering tendency on both the FE and magnetic subsystems, and hence reduces the entropy in both. This will result in a magnetic contribution to the ECE, referred to as cross caloric [7]. The caloric response is quantified by the isothermal entropy change under field application or removal. From the free energy in Eq. (1), the entropy at a given temperature and field E is $S(T,E) = -(\partial\mathcal{F}/\partial T)_E$, while the entropy change when increasing the field from 0 to E is [7,29] $\Delta S(T,E) = S(T,E) - S(T,0) = -\frac{1}{2}\alpha_P[P^2(T,E) - P^2(T,0)] - \frac{1}{2}\alpha_q[M_q^2(T,E) - M_q^2(T,0)]$. Here, the first term is the usual ECE, while the second term is the magnetic contribution, i.e., the cross-caloric response.

Figures 3(a)–3(c) show the isothermal entropy change in $SrMnO_3$ as a function of temperature for an applied field of 150 kV/cm, at the three strain values discussed previously. The total entropy change has been decomposed in magnetic and electric contributions. The total caloric response exhibits features (peaks and/or kinks) at all critical temperatures (with or without field). Generally, the electric contribution is nonzero at all temperatures and peaks at the zero field T_c^P. Below, but near $T_c^C(E)$, it is enhanced compared to the case without ME coupling. For $\eta = 2.8\%$ this even leads to an additional peak at $T_c^C(0)$. Hence, the ME coupling can enhance the ECE not only by adding the magnetic cross-caloric effect, but also by enhancing the electric part. The magnetic contribution vanishes above $T_c^C(E)$, but rises sharply between $T_c^C(E)$ and $T_c^C(0)$, peaking at $T_c^C(0)$, then slowly decreases again towards lower T, except for the case of $\eta = 2.5\%$, where it peaks at T_c^P. This is related to the kink in $M_C(T)$ at this temperature for zero field [see Fig. 2(b)]. The inset in Fig. 3(b) shows the magnetic and electric contributions to the entropy change at $\eta = 2.63\%$ and temperatures 140 and 162 K, as functions of applied electric field, illustrating an approximately linear increase in the magnitude of the entropy change with the field.

Strikingly, at all three strains, the magnetic contribution reaches approximately 60% of the electric contribution, or more than a third of the total entropy change. This is a result of particular relevance, since it shows that such a *giant* ME cross-caloric effect can significantly increase the caloric response suitable for solid state cooling. Furthermore, the effect is of similar size for the three different strains, indicating that a very careful tuning of the two critical temperatures to coincide is not necessary. It is also interesting that, in the case of $\eta = 2.8\%$, the largest total ECE is not obtained at the FE phase transition, but at the magnetic one. This is because it is the lower temperature phase transition in this case and thus the two contributions add up, while at the FE transition the magnetic contribution vanishes.

Another instructive quantity to characterize caloric effects is the adiabatic temperature change ΔT, which can be estimated from the entropy change ΔS via $\Delta T = -(T/C_{\mathrm{ph}})\Delta S$, where C_{ph} is the phonon specific heat, without the contribution of the FE degrees of freedom [29,49]. We use the temperature dependent phonon specific heat obtained for $SrMnO_3$ using frozen phonon calculations [29,50], which also contains contributions of the phonon modes responsible for the ferroelectricity and thus will slightly underestimate ΔT. The resulting ΔT is plotted in Fig. 3(d), for the same strains as in (a)–(c), and three different applied fields. The largest ΔT, for $E = 200$ kV/cm, is about 5 K. This is of the order of magnitude needed to be technologically relevant and of similar size as the "giant" ECE reported by Mischenko *et al.* [51] for $PbZr_{0.95}Ti_{0.05}O_3$, when compared at the same applied field strength (~4.5 K at 180 kV/cm in Ref. [51]). Although being estimates, the temperature changes in Fig. 3(d) show that multiferroic perovskite oxides can indeed be of potential technological relevance within the area of solid state cooling.

In summary, we have used a Landau theory, allowing several magnetic order parameters to couple to a FE polarization, to study ME coupling phenomena around

the TCP appearing in the strain-temperature phase diagram of $SrMnO_3$. Since all parameters entering the theory have been determined from first principles DFT-based calculations, realistic materials specific predictions can be made without experimental input. The ME coupling is found to be enhanced at the TCP and a huge response to electric fields is observed in the magnetic order parameter. Investigating the ECE, we find a large cross-caloric contribution due to the electric-field-induced magnetic entropy change, resulting in an increase of about 60% in the total caloric response. This provides a new way for greatly enhancing caloric effects for solid state cooling applications, by using multiferroic materials with coupled magnetic and electric order parameters. It also provides a unique example where AFM order in a multiferroic material can be of great practical usefulness. Recent work proving that highly strained multiferroic films of $SrMnO_3$ can be grown [24] is promising regarding the experimental verification of these results, while similar studies on Ba-doped systems [44,52,53] would also be of interest. Further insights could also be obtained by studies using other computational methods, e.g., based on microscopic models for coupled spin-lattice dynamics [43,54].

A. E. is grateful to Quintin Meier for discussions. This work was supported by the Swiss National Science Foundation (Project Code 200021E-162297) and the German Science Foundation under the priority program SPP 1599 ("Ferroic Cooling"). Computational work was performed on resources provided by the Swiss National Supercomputing Centre (CSCS).

[1] S. Fähler, U. K. Rössler, O. Kastner, J. Eckert, G. Eggeler, H. Emmerich, P. Entel, S. Müller, E. Quandt, and K. Albe, Adv. Eng. Mater. **14**, 10 (2012).
[2] X. Moya, S. Kar-Narayan, and N. D. Mathur, Nat. Mater. **13**, 439 (2014).
[3] E. Stern-Taulats, T. Castán, L. Mañosa, A. Planes, N. D. Mathur, and X. Moya, MRS Bull. **43**, 295 (2018).
[4] M. M. Vopson, Solid State Commun. **152**, 2067 (2012).
[5] H. Meng, B. Li, W. Ren, and Z. Zhang, Phys. Lett. A **377**, 567 (2013).
[6] S. Anand and U. V. Waghmare, Mater. Res. Express **1**, 045503 (2014).
[7] A. Planes, T. Castan, and A. Saxena, Philos. Mag. **94**, 1893 (2014).
[8] S. Lisenkov, B. K. Mani, C.-M. Chang, J. Almand, and I. Ponomareva, Phys. Rev. B **87**, 224101 (2013).
[9] Y. Liu, G. Zhang, Q. Li, L. Bellaiche, J. F. Scott, B. Dkhil, and Q. Wang, Phys. Rev. B **94**, 214113 (2016).
[10] Y.-Y. Gong, D.-H. Wang, Q.-Q. Cao, E.-K. Liu, J. Liu, and Y.-W. Du, Adv. Mater. **27**, 801 (2015).
[11] J. Liu, T. Gottschall, K. P. Skokov, J. D. Moore, and O. Gutfleisch, Nat. Mater. **11**, 620 (2012).
[12] E. Mendive-Tapia and T. Castán, Phys. Rev. B **91**, 224421 (2015).
[13] Y. Liu, L. C. Phillips, R. Mattana, M. Bibes, A. Barthélémy, and B. Dkhil, Nat. Commun. **7**, 11614 (2016).
[14] T. Gottschall, A. Gràcia-Condal, M. Fries, A. Taubel, L. Pfeuffer, L. Mañosa, A. Planes, K. P. Skokov, and O. Gutfleisch, Nat. Mater. **17**, 929 (2018).
[15] C. Cazorla and J. Íñiguez, Phys. Rev. B **98**, 174105 (2018).
[16] N. A. Spaldin, S.-W. Cheong, and R. Ramesh, Phys. Today **63**, No. 10, 38 (2010).
[17] N. A. Spaldin and R. Ramesh, Nat. Mater. **18**, 203 (2019).
[18] We use the terminology of Ref. [7], that a multicaloric effect is the result of applying or removing multiple fields, additional to the sum of applying/removing each field separately. The caloric response in one ferroic property due to the field conjugate to another ferroic property coupled to the first one is called a cross-caloric effect.
[19] L. D. Landau, E. M. Lifshitz, and L. P. Pitaevskii, in *Statistical Physics—Part 1*, 3rd ed. (Pergamon Press, Oxford, England, 1980), Vol. 4, p. 10.
[20] A. Edström and C. Ederer, Phys. Rev. Mater. **2**, 104409 (2018).
[21] J. H. Lee and K. M. Rabe, Phys. Rev. Lett. **104**, 207204 (2010).
[22] C. Becher, L. Maurel, U. Aschauer, M. Lilienblum, C. Magé, D. Meier, E. Langenberg, M. Trassin, J. Blasco, I. P. Krug, P. A. Algarabel, N. A. Spaldin, J. A. Pardo, and M. Fiebig, Nat. Nanotechnol. **10**, 661 (2015).
[23] R. Guzman, L. Maurel, E. Langenberg, A. R. Lupini, P. A. Algarabel, J. A. Pardo, and C. Magen, Nano Lett. **16**, 2221 (2016).
[24] J. W. Guo, P. S. Wang, Y. Yuan, Q. He, J. L. Lu, T. Z. Chen, S. Z. Yang, Y. J. Wang, R. Erni, M. D. Rossell, V. Gopalan, H. J. Xiang, Y. Tokura, and P. Yu, Phys. Rev. B **97**, 235135 (2018).
[25] T. Takeda and S. Ōhara, J. Phys. Soc. Jpn. **37**, 275 (1974).
[26] J. H. Lee and K. M. Rabe, Phys. Rev. B **84**, 104440 (2011).
[27] S. Kamba, V. Goian, V. Skoromets, J. Hejtmánek, V. Bovtun, M. Kempa, F. Borodavka, P. Vaněk, A. A. Belik, J. H. Lee, O. Pacherová, and K. M. Rabe, Phys. Rev. B **89**, 064308 (2014).
[28] E. O. Wollan and W. C. Koehler, Phys. Rev. **100**, 545 (1955).
[29] See Supplemental Material at http://link.aps.org/supplemental/10.1103/PhysRevLett.124.167201 for a detailed discussion regarding the determination of the parameters for the Landau theory, which additionally includes Refs. [30–39].
[30] G. Kresse and J. Hafner, Phys. Rev. B **47**, 558 (1993).
[31] G. Kresse and J. Hafner, Phys. Rev. B **49**, 14251 (1994).
[32] G. Kresse and J. Furthmüller, Comput. Mater. Sci. **6**, 15 (1996).
[33] P. E. Blöchl, Phys. Rev. B **50**, 17953 (1994).
[34] G. Kresse and D. Joubert, Phys. Rev. B **59**, 1758 (1999).
[35] J. P. Perdew, A. Ruzsinszky, G. I. Csonka, O. A. Vydrov, G. E. Scuseria, L. A. Constantin, X. Zhou, and K. Burke, Phys. Rev. Lett. **100**, 136406 (2008).
[36] S. L. Dudarev, G. A. Botton, S. Y. Savrasov, C. J. Humphreys, and A. P. Sutton, Phys. Rev. B **57**, 1505 (1998).
[37] E. Şaşıoğlu, L. M. Sandratskii, and P. Bruno, Phys. Rev. B **70**, 024427 (2004).

[38] P. W. Anderson, in *Solid State Physics*, Vol. 14, edited by F. Seitz and D. Turnbull (Academic Press, New York, 1963), pp. 99–214.
[39] R. Søndenå, S. Stølen, P. Ravindran, and T. Grande, Phys. Rev. B **75**, 214307 (2007).
[40] The microscopic effective Hamiltonian results of Ref. [20] are not directly comparable to the results presented here, due to the differences in how the coupling between magnetism and ferroelectricity is considered.
[41] L. Maurel, N. Marcano, T. Prokscha, E. Langenberg, J. Blasco, R. Guzmán, A. Suter, C. Magén, L. Morellón, M. R. Ibarra, J. A. Pardo, and P. A. Algarabel, Phys. Rev. B **92**, 024419 (2015).
[42] We note that the difficulty in treating ME coupling with only lowest order terms might also have important implications for other methods describing coupled dynamics between spin and lattice degrees of freedom, such as, e.g., described in Ref. [43].
[43] J. Hellsvik, D. Thonig, K. Modin, D. Iuşan, A. Bergman, O. Eriksson, L. Bergqvist, and A. Delin, Phys. Rev. B **99**, 104302 (2019).
[44] H. Sakai, J. Fujioka, T. Fukuda, D. Okuyama, D. Hashizume, F. Kagawa, H. Nakao, Y. Murakami, T. Arima, A. Q. R. Baron, Y. Taguchi, and Y. Tokura, Phys. Rev. Lett. **107**, 137601 (2011).
[45] G. Giovannetti, S. Kumar, C. Ortix, M. Capone, and J. van den Brink, Phys. Rev. Lett. **109**, 107601 (2012).
[46] The precise critical exponents would of course be altered in a theory correctly considering fluctuations.
[47] H. Wiegelmann, A. G. M. Jansen, P. Wyder, J.-P. Rivera, and H. Schmid, Ferroelectrics **162**, 141 (1994).
[48] J. Íñiguez, Phys. Rev. Lett. **101**, 117201 (2008).
[49] A. Grünebohm, Y.-B. Ma, M. Marathe, B.-X. Xu, K. Albe, C. Kalcher, K.-C. Meyer, V. V. Shvartsman, D. C. Lupascu, and C. Ederer, Energy Technology **6**, 1491 (2018).
[50] A. Togo and I. Tanaka, Scr. Mater. **108**, 1 (2015).
[51] A. S. Mischenko, Q. Zhang, J. F. Scott, R. W. Whatmore, and N. D. Mathur, Science **311**, 1270 (2006).
[52] H. Somaily, S. Kolesnik, J. Mais, D. Brown, K. Chapagain, B. Dabrowski, and O. Chmaissem, Phys. Rev. Mater. **2**, 054408 (2018).
[53] L. Maurel, N. Marcano, E. Langenberg, R. Guzmán, T. Prokscha, C. Magén, J. A. Pardo, and P. A. Algarabel, APL Mater. **7**, 041117 (2019).
[54] I. A. Kornev, S. Lisenkov, R. Haumont, B. Dkhil, and L. Bellaiche, Phys. Rev. Lett. **99**, 227602 (2007).